Applied Catalysis B: Environmental 181 (2016) 228–235

Contents lists available at ScienceDirect

Applied Catalysis B: Environmental

journal homepage: www.elsevier.com/locate/apcatb

Modelling of Carbon Black oxidation in the presence of CeO_2 catalyst using a 3D representation of the solid–solid mixture

May Issa, Alain Brillard*, Valérie Tschamber, Jean-François Brilhac

Laboratoire Gestion des Risques et Environnement (EA2334), Université de Haute-Alsace, 3bis rue Alfred Werner, 68093 Mulhouse, France

ARTICLE INFO

Article history:
Received 30 April 2015
Received in revised form 20 July 2015
Accepted 24 July 2015
Available online 29 July 2015

Keywords:
Soot oxidation modelling
Carbon Black–ceria mixture
3D representation of mixtures
Determination of kinetic parameters

ABSTRACT

A model based on a 3D representation of mixtures involving Carbon Black (CB) and commercial ceria (CeO_2) particles placed in a fixed bed reactor is proposed. Catalyst particles may aggregate in different ways in the whole bed and different CB–CeO_2 mass ratios are considered which range from 95–5 to 10–90. Two types of oxidation are assigned by the model: a catalytic oxidation under the influence of CeO_2 and a non-catalytic one in the other case. The activation energies of these oxidation processes have been determined through experiments, while their frequency factors are derived for the two reactions using a numerical simulation. The model simulates the CB oxidation in a good way whatever the CB–CeO_2 mass ratio, except for the 50–50 case. The catalytic oxidation is here underestimated, as the contact between CB and CeO_2 is progressively lost.

© 2015 Elsevier B.V. All rights reserved.

1. Introduction

Soot particles and NO_x are the main undesired by-products emitted by Diesel engines. Soot particles consist of a carbon structure with inorganic material and adsorbed hydrocarbons – SO_x and water – and are composed of single particles of few nanometers agglomerated in entities with a typical size in the range 0.1–10 μm [1]. Diesel particulate filters (DPF) are used for soot removal from gas stream. DPF are wall-flow monoliths with a honeycomb structure where soot particles are stuck on the walls, the gas flowing through the porous wall. Once soot is collected in the DPF, different regeneration strategies may be adopted [2,3]: (i) the continuously regenerating trap, mainly using NO_2 as oxidant, (ii) fuel borne catalyst, enhancing the oxidation of the catalyzed filtered soot, (iii) post-injection of fuel for temperature rise. DPF are coated with catalyst to ensure the filter regeneration through an oxidation process of the collected soot. Different catalytic active phases are always under investigation, among them oxide catalysts, e.g. V_2O_5 [4], Fe_2O_3 [2] and CeO_2. CeO_2 and TiO_2 supported precious metal (Ag, Pt and Pd) catalysts are also proposed for soot oxidation [5]. The ceria-based catalysts are among the most promising phases in substitution to noble metals [6]. The catalytic performance of ceria based material for soot combustion is directly linked to the redox properties of Ce^{3+}/Ce^{4+} (see [7,8]) and to the capacity of cerium oxide to exchange oxygen with the bulk gas [9] and the catalyst particle size [10]. Cerium oxide exhibits large deviations from its CeO_2 stoichiometric composition in a reducing atmosphere, with a general formula CeO_{2-x}, where $0 \leq x \leq 0.5$. In the presence of oxygen, these compounds are easily re-oxidized to CeO_2 at room temperature (see [11]). Fornasiero et al. reported in [12] that the reduction of CeO_2 is a slow process in comparison to CeO_{2-x} oxidation. Boaro et al. showed in [13] that the degree of ceria reduction does not exceed 5% in the temperature range 553–773 K under CO. For the catalyst screening, commercial Carbon Blacks are used as soot model, as they are less heterogeneous than real soot. A number of mechanisms for carbon oxidation by catalysts were proposed in Ref. [9], among which is the redox mechanism which consists in carbon oxidation by lattice oxygen from the catalyst and re-oxidation of the catalyst by oxygen from the gas phase. The study [14] performed by De Soete revealed that oxidant adsorption is generally much faster on metal sites than on carbon sites. This author reported that the enhancement of the carbon combustion in the presence of catalyst is due to the fact that carbon adsorbs metal bound oxygen atoms faster than molecular oxygen. Furthermore, Stratakis and Stamatelos investigated in [15] the soot oxidation reaction in the presence of fuel additive containing an organometallic ceria compound. The mechanism of soot ceria-catalyzed combustion by O_2 is the so-called 'active oxygen mechanism' [6]. Ceria exchanges its oxygen with the oxygen present in the bulk gas, through complex reactions, and during this exchange process reactive species – active oxygen – are created which can oxidize soot. Hence the active oxygen soot combustion depends on the soot–ceria contact. The activity of the oxidation catalysts for soot combustion is mainly investigated

* Corresponding author.
E-mail address: Alain.Brillard@uha.fr (A. Brillard).

http://dx.doi.org/10.1016/j.apcatb.2015.07.040
0926-3373/© 2015 Elsevier B.V. All rights reserved.

by means of a temperature programmed oxidation (TPO) process which can be carried out by TGA or in a fixed bed reactor [16]. A challenging aspect to be considered for catalytic soot combustion is how to mimic such a contact in laboratory experiments with powder catalyst. This contact has been studied in the literature by many authors, see [17] and the references therein. Two types of contact are usually explored [18]: (i) loose contact, for which the catalyst-carbon mixture is prepared using a spatula and (ii) tight contact, obtained through an intimate milling of the two solids. Many physico-chemical experiments and studies have been performed which are focused on the characterization of the contact between soot and catalyst particles [16,19]. Different catalysts were tested considering the influence of both the shape and the material which is used as catalyst, in order to obtain the better activity or efficiency for soot oxidation [18]. Recent investigations analyze the impact of ceria-based catalysts morphologies (fibres, sticks, flakes, stars) on soot oxidation [18,20–22]. These works investigate the properties of the catalyst at a particle level. They aim at enhancing the number of possible contacts between soot and catalyst. It emerges that ceria nanofibres present a relevant morphology due to the network of fibres which surround the soot particles [18]. The particle size also plays a key role in soot combustion and a recent work [10] proves a linear dependence between catalyst particle size and soot combustion capacity.

Modelling soot oxidation and determining the kinetic parameters of this reaction have already been the subject of many papers in the literature, see the review paper [23] and also [2,24]. These papers or even the models which have already been developed intend to describe the phenomena occurring during soot deposition [25], soot oxidation and filter regeneration [3,26], but without taking into account the contact between the soot and catalyst particles. Therefore, the aim of the present work is to propose a model based on a 3D representation of mixtures involving Carbon Black (CB) and commercial ceria (CeO_2) particles and which simulates the CB oxidation process which occurs in a fixed bed reactor. The CB oxidation model which is presented here allows extracting the kinetic parameters of CB oxidation within this context.

2. Experimental setting

2.1. Materials and characterization

A commercial CB (Vulcan 6 from Cabot Company) has been used in this study. The elementary analysis of the samples is the following: C: 95.3%, H: 1.2%, N: 0.3%, O: 1,9%, S: 1% and N < 0.3% in weight (a CB sample has been oxidized up to 1050 °C under a He/O_2 atmosphere in a microanalyzer. C, H, N and S are converted in CO_2, H_2O, NO/NO_2 and SO_2, respectively, and measured by specific detectors, while O is estimated by difference). A commercial ceria (CeO_2) purchased from Rhodia Company (purity 99.9%) has been used as catalyst. Cerium is assumed to exist mainly under its oxidized form [15].

The specific CeO_2 surface area was estimated using a Micromeritics ASAP 2010. A XRD characterization was performed using a diffractometer Philips Panalytical X'Pert Pro MPD theta. From BET theory, a specific surface area of 120 m^2/g is obtained for CeO_2 as received. A significant decrease of the specific surface area was observed after grinding this sample during 15 min (86 m^2/g instead of 120 m^2/g). Such a behaviour may be explained by the agglomeration of small CeO_2 particles during the grinding step as previously reported by Rougier et al. [27]. A X-ray diffraction pattern for cerium oxide presented in Ref. [28] shows a face cubic centred crystal structure with a fluorine type (Fm-3m), where each cerium cation is associated to eight oxygen anions. The lattice parameters are $a = b = c = 5.41$ nm.

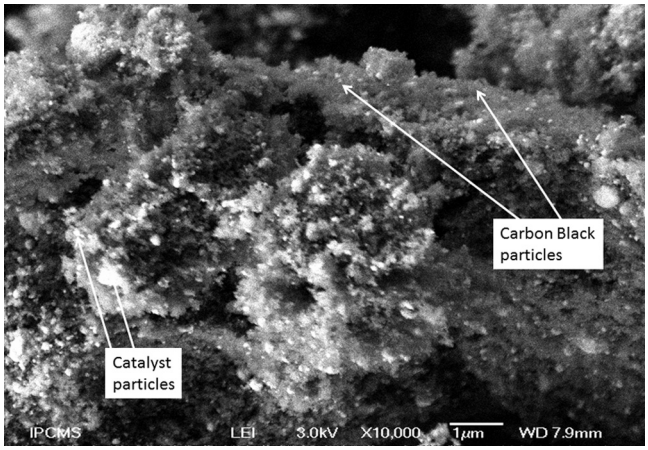

Fig. 1. Picture of mixture cerium oxide sieved then milled with CB for a 50–50 ratio mixture. Catalyst (resp. CB) particles are the white (resp. grey) ones.

Different CB–CeO_2 mixtures were tested for oxidation in a fixed bed reactor (mass ratio CB–CeO_2 ranging from 5–95 to 95–5, with a total mass of the sample approximately equal to 5 mg) in order to get a better understanding of the effect of CB–CeO_2 ratio on CB oxidation. In the following, notice that in the presentation of a CB–CeO_2 mixture, we will always write first the mass proportion of CB and then that of CeO_2. All the samples were prepared with the following procedure: first grinding during 3 min, then sieving of CeO_2 (36–40 μm) and finally grinding of ceria with CB during 15 min. Such a procedure leads to an intimate mixture of soot and powder catalyst which has been previously defined as tight contact. Even if in a real catalytic filter the soot–catalyst contact is assumed to be loose or poor [17], it is better from a practical point of view to obtain catalytic results with samples exhibiting a tight contact between CB and catalyst, in order to enhance the effect of the contact for the different CB–CeO_2 ratio samples which have to be tested. Moreover, loose contact mixtures were previously investigated in our laboratory (see [16,28]). No significant effect of the presence of CeO_2 on CB oxidation was found in a loose type mixture (see [16]). This means that the CeO_2 catalyst which has been used for this study is not efficient enough for CB oxidation to occur in loose contact conditions because of the size distribution of the catalyst particles.

The samples were observed by scanning electron microscopy with a JEOL JSM-6700 F microscope in order to study the morphology of the CB–CeO_2 mixtures and to define a 3D representation of the medium. A SEM picture of a 50–50 mixture is shown in Fig. 1 (more pictures have already been presented in Refs. [16,28]).

This picture exhibits granulated areas identified as CeO_2, which appear as aggregated grains and the ultimate CeO_2 grains are in the 50–80 nm range [16]. CeO_2 aggregates are surrounded by CB zones characterized by their foamy aspect. Quite similar electron micrograph pictures were recently presented by Vernikovskaya et al. in [26], the soot here building a layer on the top of fibre quartz noncatalytic fibres.

2.2. Investigation of the CB oxidation process

A gas mixture 10% O_2/90% N_2 flew across the fixed bed reactor (total gas flow rate of 40 NL/h). Experiments were performed under isothermal conditions (425–600 °C) or under a temperature programmed oxidation process (TPO with a heating rate of 10 °C/min). A more detailed description of the experimental set-up is given in Ref. [16]. The CB oxidation rate was computed from CO and CO_2 mole fractions measured at the reactor outflow by an infrared analyzer (COSMA Cristal 300), see Fig. 2.

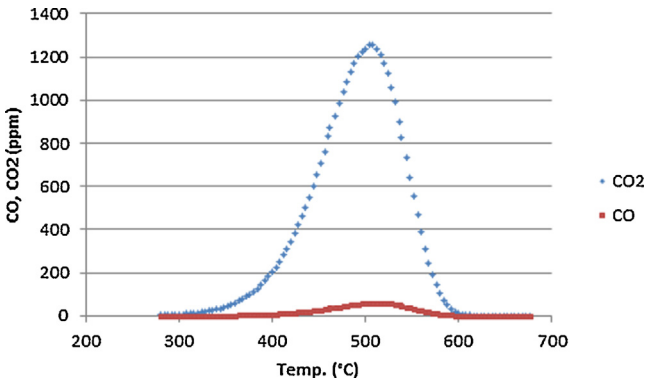

Fig. 2. CO and CO_2 emission lines for a 50–50 mixture prepared as above-described.

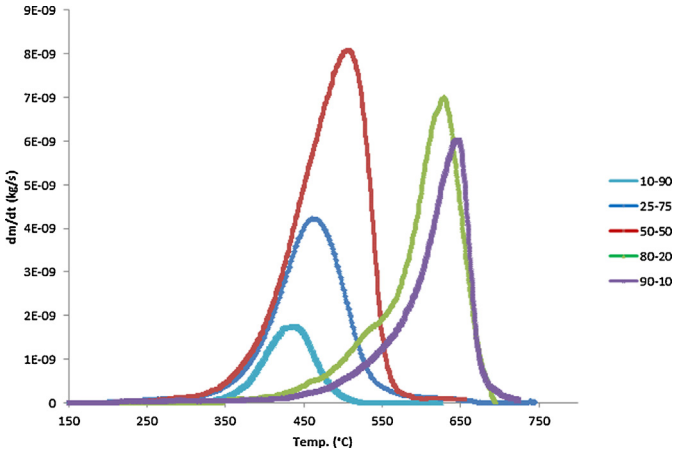

Fig. 3. Mass loss rate curves for different ratio mixtures.

The gas temperature was measured with a thermocouple (type K) located above the sample. Carbon oxidation rate versus temperature is plotted in Fig. 3, for samples presenting different mass ratios.

The CB oxidation process in the presence of a small amount of CeO_2 (mixture 95–5) starts at 350°C and reaches a maximum intensity at around 645 °C. In the presence of a high catalyst mass fraction in the sample (10–90), the CB oxidation process slowly starts at slightly lower temperatures (300 °C) and reaches a maximum intensity at 425 °C. An increase of the CeO_2 mass fraction strongly improves the rate of CB oxidation: CB oxidation indeed starts at 300 °C and reaches a maximum at 625 °C for 80–20, 500 °C for 50–50 and 450 °C for 25–75.

3. Representation of the mixture

From the visual analysis of the SEM picture, see Fig. 1, the mixture may be considered as a stacking of CB and CeO_2 isometric volumes. We performed measurements on an Electrical Low Pressure Impactor (ELPI, Dekati Ltd) in order to determine a particle size distribution of the ceria. It appears that 75% of ceria particles are in the range 264–953 nm, 11% in the range 95–264 nm and 14% are larger than 953 nm, see [16]. We may accordingly assume that the characteristic length of the isometric volumes is 200 nm. It corresponds to the size of the smallest group of CeO_2 single-crystalline, as observed from microscopy (see Fig. 1) and measured by ELPI.

The size of the bed considered in the present study for modelling is $10 \times 10^{-6} \times 10 \times 10^{-6} \times 3 \times 10^{-6}$ m^3 and is filled in with $50 \times 50 \times 15 = 37\,500$ cubic cells each of them having a length equal

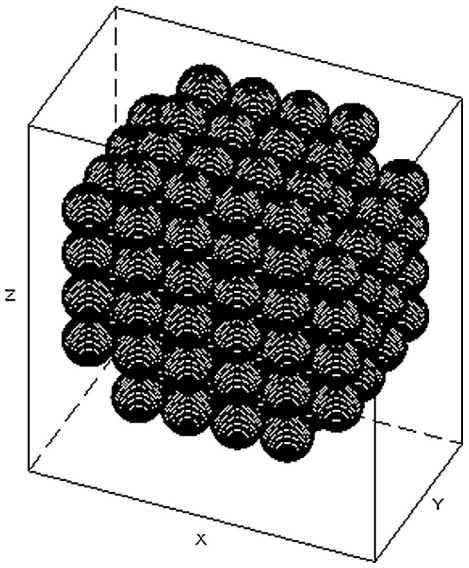

Fig. 4. 3D representation of a catalyst aggregate of 1200 nm maximal length (6 layers).

to 0.2×10^{-6} m = 200 nm and containing either a catalyst or a CB particle.

The density of the ceria is taken as 1.188×10^3 kg m^{-3}, while that of CB is taken as 3.12×10^2 kg m^{-3}. With these values, the following distribution of CB and catalyst particles in the bed are obtained (see Table 1) according to the different CB–catalyst ratios.

For example, in the case of 95–5 CB–CeO_2 mass ratio, let n_{CB} (resp. n_C) be the number of CB (resp. catalyst) particles. We have the following equations related to the overall number of particles in the bed or to the CB–CeO_2 mass ratio under consideration

$$\begin{cases} n_{CB} + n_C = 37\,500, \\ 312 n_{CB} = \dfrac{95}{5} 1188 n_C, \end{cases}$$

which implies $n_{CB} = 19 \times 1188/312 n_C$ and $n_C = 37\,500 \times 312/(19 \times 1188 + 312) = 511$. Then $n_{CB} = 19 \times 1188/312 \times 511 = 36\,989$.

In the 3D bed, the catalyst particles may be either isolated or assembled through aggregates, as suggested by the SEM observations. According to the ELPI measurements [16], we will consider three types of catalyst aggregates, all of them being given an oblong shape with a maximal length of 400, 800 or 1200 nm and obtained when gathering 2, 4 or 6 layers of catalyst particles, respectively. Table 2 gives the number of catalyst particles building each kind of catalyst aggregates.

Fig. 4 presents the structure of a model catalyst aggregate with a maximal length of 1200 nm, thus containing 128 particles. It is composed of six layers containing 24 cells and of two layers containing 16 particles at both ends of the aggregate. Each cell is filled in with a catalyst particle.

The overall number of catalyst particles (isolated or assembled as aggregates) in the bed depends on the CB–CeO_2 mass ratio. Table 3 gives the numbers of catalytic aggregates and of isolated catalyst particles considered in the 3D bed for the different CB–CeO_2 mass ratios which have been tested (remember that the number of catalyst particles is given in each aggregate in Table 2). These numbers have been determined considering the proportions of the different aggregates present in the samples according to their maximal size, as observed by microscopy.

The catalyst aggregates are randomly placed in the whole bed. The further isolated catalyst particles are randomly placed in the

Table 1
Number of CB and catalyst particles depending on the CB–CeO_2 mass ratio.

Mixture ratio	95–5	80–20	50–50	25–75	10–90
Number CB particles	36 989	35 190	29 700	20 975	11 149
Number catalyst particles	511	2310	7800	16 525	26 351

Table 2
Number of layers and catalyst particles building each kind of catalyst aggregate.

Length of the aggregate (nm)	No. of layers	No. of catalyst particles
400	2	6
800	4	32
1200	6	128

Table 3
Number of catalyst aggregates considered to build each 3D bed (depending on the CB–CeO_2 mass ratios).

Length of the aggregates	95–5	80–20	50–50	25–75	10–90
200 nm (isolated particle)	3	12	30	143	7391
400 nm	10	47	159	357	600
800 nm	6	27	93	205	200
1200 nm	2	9	30	60	70

remaining free places of the whole bed. Once all the catalyst particles have been placed in the bed, the CB particles are placed in the free remaining places of the overall bed. One exception to this random distribution of the different kinds of catalyst aggregates is the case of samples with a high catalyst ratio (10–90). In that case, the number of catalyst aggregates to be placed in the bed is so high (see Table 3) that it is not possible to proceed in such a way. We instead put in a random way the appropriate number of CB particles in the bed previously totally filled in with catalyst particles.

4. Description of the soot oxidation model

4.1. Model assumptions

The model assumes a pseudo steady-state regime, an uniform gas flow rate, isothermal conditions in the bed and a thermal equilibrium between the solid and the gas. The heat released by the oxidation reaction is neglected. In our experiments, the gas convective flow is crossing the packed bed of CeO_2/CB mixture deposited. We thus assume that there is no diffusional limitation for oxygen transport from the bulk gas to the reacting solid surface. Under the influence of the catalyst particles, the CB particles may burn due to the presence of an oxidative and heated environment. Moreover, CB oxidation without any catalytic effect has to be considered, as some CB particles are located far from catalyst particles, especially when the catalyst mass ratio is low. For simplicity, the description of the influence of catalyst particles on a CB particle is presented considering only a section of the bed, i.e. a 2D representation (see Fig. 5). The dark particles represent CB ones and the yellow ones correspond to ceria. In the case of Fig. 5c, the circled CB particle is almost totally surrounded by catalyst particles. The CB oxidation is here surely a catalytic one, because the CB particle is located in the field of influence of catalyst particles. In the case of Fig. 5a, the circled CB particle is surrounded by a lower number of catalyst particles (in this 2D representation). The influence of the catalyst particles is surely lower than in the case of Fig. 5c). But we can still here consider a catalytic oxidation. In Fig. 5b, the circled CB particle is totally surrounded by other CB particles. The influence of catalyst particles is much lower than for the preceding cases. CB oxidation should here be considered as a non-catalytic one.

According to this representation, a distinction must be made between two types of soot oxidation for each CB particle, according

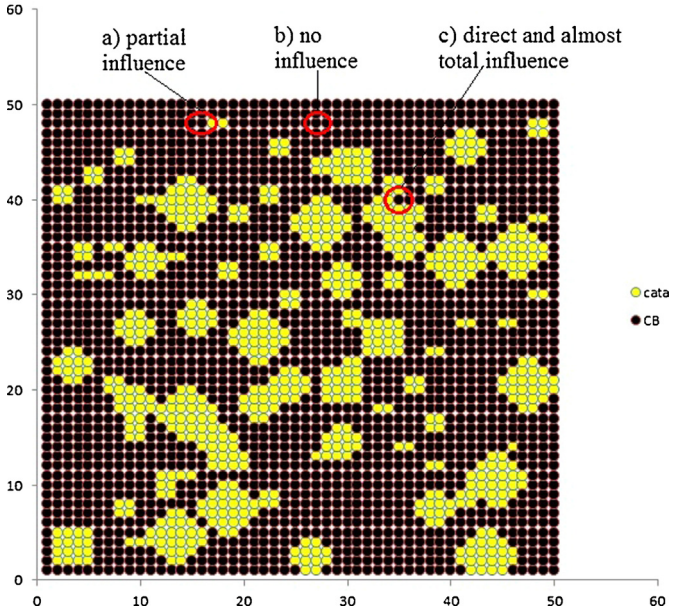

Fig. 5. Analysis of the influence of catalyst particles on CB particles (repartition of catalyst and CB particles in the case of 50CB–50CeO_2 mass ratio). (For interpretation of the references to colour in this figure text, the reader is referred to the web version of this article.)

to the distance between this CB particle and the catalyst particles present in the bed:

- CB particles which are in tight contact with CeO_2 and which are burnt away through a catalyzed reaction at low temperatures:

$$(-C) + 2CeO_2 \mapsto CO_2 + 2Ce_2O_3$$

- CB particles for which CB oxidation does not depend on the influence of the catalyst particles (only reaction between CB and molecular oxygen):

$$2(-C) + \frac{3}{2}O_2 \mapsto CO_2 + CO$$

In our model, the influence of the jth catalyst particle on the ith CB particle involves the distance d_{ij} between this ith CB particle and the jth catalyst particle. The distance between two neighbouring particles (in fact between the centres of these particles) takes one of the following three values, depending on their corresponding positions (see Fig. 5):

- if the cubes containing the two particles share a face, the distance between the particles is equal to the distance a between their centres (a = 200 nm),
- if the cubes containing the two particles share an edge, the distance between the particles is equal to $a\sqrt{2}$,
- if the cubes containing the two particles are in contact only through a summit, the distance between the particles is equal to $a\sqrt{3}$.

For the catalytic oxidation of a CB particle to occur, we will only consider the case where one or many catalyst particles are located at most at a distance $a\sqrt{3}$ of this CB particle. This means that we only take into account the close neighbours of a CB particle (at least sharing a summit of the cubic cells where they are placed) for a catalytic oxidation process to occur. The influence of these catalyst particles is then taken into account through the inverse of their distance to the CB particle.

4.2. Catalytic soot oxidation rate

When a catalytic oxidation occurs for the ith CB particle, under the influence of neighbouring catalyst particles, the mass loss rate of this CB particle evolves with respect to the time parameter t according to the first-order reaction law

$$\frac{dm_i}{dt}(t) = -\sum_{j=1}^{n(i)} k(T(t))\frac{1}{d_{ij}} m_i(t) \tag{1}$$

where $m_i(t)$ is the mass of the ith CB particle at time t, d_{ij} is the Euclidean distance between the centre (x_i, y_i, z_i) of the ith CB particle and that (x_j, y_j, z_j) of the jth catalyst particle given by

$$d_{ij} = \sqrt{\left(x_i - x_j\right)^2 + \left(y_i - y_j\right)^2 + \left(z_i - z_j\right)^2}.$$

In (1), the sum is extended to the number $n(i)$ of close neighbouring (at least sharing a summit) catalyst particles of the ith CB particle and $k(T)$ is the kinetic constant whose expression obeys an Arrhenius law

$$k(T) = k_0 \exp(-Ea/RT),$$

where k_0 (resp. Ea) is the frequency factor expressed in m s^{-1} (resp. the activation energy), R is the gas constant ($R = 8.314$ J mol^{-1} K^{-1}) and T is the temperature (K).

In (1), one may observe that the oxidation rate of the ith CB particle is proportional to the inverse of the distance d_{ij} between the centres of the ith CB particle and of the neighbouring jth catalyst particle.

Eq. (1) is completed with the initial condition $m_i(t) = m_0$, the initial mass of the ith CB particle of diameter 200 nm.

4.3. Non-catalytic soot oxidation rate

For the ith CB particle which is not in tight contact with at least one catalyst particle, a non-catalytic oxidation reaction is considered which is associated to the first-order expression of the mass loss rate

$$\frac{dm_i}{dt}(t) = -k'(T(t))(m_i(t))^{\alpha}, \tag{2}$$

where $m_i(t)$ is the mass of the ith CB particle at time t and $k'(T)$ obeys an Arrhenius form

$$k'(T) = k'_0 \ \exp\left(-\frac{E'a}{RT}\right),$$

where k'_0 is the frequency factor expressed in kg$^{1-\alpha}$ s^{-1} and $E'a$ is the activation energy for this non-catalytic oxidation. Here α is a fitted parameter which will be taken equal to 0.67, see [28].

Eq. (2) is again completed with the initial condition $m_i(t) = m_0$, the initial mass of the ith CB particle of diameter 200 nm.

The global mass (and mass loss rate) of the CB present in the bed is the sum of all the mass (and mass loss rates) given through either (1), in the case of a catalytic reaction, or (2), in the case of a non-catalytic reaction

$$\begin{cases} \dfrac{dm}{dt}(t) = \displaystyle\sum_{i=1}^{n_{CB}} \frac{dm_i}{dt}(t), \\ m(t) \quad = \displaystyle\sum_{i=1}^{n_{CB}} m_i(t), \end{cases} \tag{3}$$

the sums being extended to the number n_{CB} of CB particles present in the bed.

4.4. The kinetic parameters to be determined

The activation energies for the catalytic ($Ea = 124.0$ kJ mol^{-1}) and non-catalytic ($E'a = 176.0$ kJ mol^{-1}) oxidation reactions are given data in our model. They have been determined through experiments, see [16,31]. These values are close to those referenced in the literature. For instance, activation energies determined using Ozawa's method [29] with and without ceria catalysts lie in the range 142–176 kJ mol^{-1}. For catalysts containing cerium, Vernikovskaya et al. returned in [26] activation energies from 160 to 85 kJ mol^{-1}, depending on the reaction order used for the remaining soot mass (0.67 and 1, respectively).

We thus only have to determine the values of the frequency factors k_0 and k'_0.

4.5. Numerical resolution

A Fortran code has been built which first places the catalyst aggregates and particles and the CB particles, as previously described, then which solves either (1) or (2), according to the position of each CB particle in comparison with that of the catalyst particles. We then optimize the values of the frequency factors using a comparison with the experimental data. More precisely, the structure of the Fortran code is the following:

- place the catalyst aggregates and particles and the CB particles, according to the above description,
- compute for each CB particle the sum of the inverse of the distances between this CB particles and the close neighbouring catalyst particles if any,
- solve either (1) or (2) for each CB particle, according to the value of the quantity determined in the preceding step, using an Euler routine and choosing initial values of the frequency factors (observe that even if it is possible to get exact solutions of (1) or (2), the expressions of these solutions involve integrals which are not easily computable),
- sum at each value of the time parameter t, the mass loss rates and the remaining mass of the CB particles in the bed, according to (3),
- optimize the choice of the frequency factors, in order to get the best agreement between the simulated and the experimental data.

5. Results and discussion

We first applied the numerical resolution presented in the above section to the 95–5 sample for the determination of the frequency factor (k'_0) corresponding to an almost non-catalytic reaction, then to a 10–90 sample for the determination of the frequency factor (k_0) associated to an almost catalytic reaction. The following values were obtained: $k_0 = 400\,000$ kg m^{-1} s^{-1} and $k'_0 = 53.2$ kg$^{1-\alpha}$ s^{-1}. Using this set of kinetic parameters, the simulated curves for the mass loss rate are then compared with the experimental ones for the different mixtures.

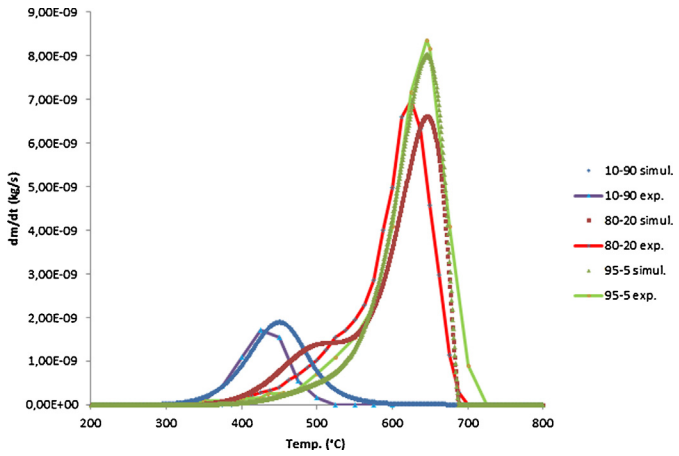

Fig. 6. The experimental and simulated mass loss rate curves for a 95CB–5CeO_2 (green) sample, for a 80CB–20CeO_2 (red) sample and for a 10CB–90CeO_2 (blue) sample. (For interpretation of the references to colour in this figure legend, the reader is referred to the web version of this article.)

5.1. The cases of 'extreme' media

Let us first consider the cases of a 95–5 ratio and of a 80–20 ratio. We here place in a random way the catalyst aggregates starting from the greater ones then going to the smaller ones. We end up with the random placement of the remaining isolated catalyst particles (according to the numbers indicated in Table 3). Then we fill in the remaining places of the bed with CB particles. As the bed is mainly composed of CB particles, the number of contacts between CB and catalyst particles is very low.

In the case of a 10–90 mass ratio, the number of catalyst particles is very high (see Table 1). Instead of placing in a random way aggregates of catalyst particles, according to Table 3, the bed is first totally filled in with catalyst particles and then the appropriate number of CB isolated particles are placed in a random way, replacing the corresponding catalyst particles.

With the above-indicated values of the kinetic constants, the corresponding simulated and experimental mass loss rate curves are gathered in Fig. 6.

In the case of a 95–5 mass ratio, the experimental and simulated mass loss rate curves are quite perfectly superposed. In the case of a 80–20 mass ratio, the experimental and simulated curves exhibit two main steps. From 400 to 500 °C, a small catalytic oxidation process described in (1) occurs. This step is quite well accounted for by the model even if it slightly overestimates the reaction rate. From 450 to 700 °C, the simulated peak which may be associated to the non-catalytic reaction described in (2) quite well corresponds to the experimental one. In the case of a 10–90 mass ratio, the curves start in the same way, but the simulated peak continues to slightly grow and ends up a little bit later.

5.2. The case of a 25–75 medium

In this case, we use the placement method described for the 90–10 mass ratio, first starting with a random placement of the large aggregates and ending with the placement of the CB particles in the remaining free places. Fig. 7 shows the location of the CB or catalyst particles and of the catalyst aggregates in the section $z = 4$ of the 3D bed in the case of a sample with a 25CB–75CeO_2 mass ratio.

With the above-indicated values of the kinetic constants, the computed and experimental mass loss rate curves are gathered in Fig. 8.

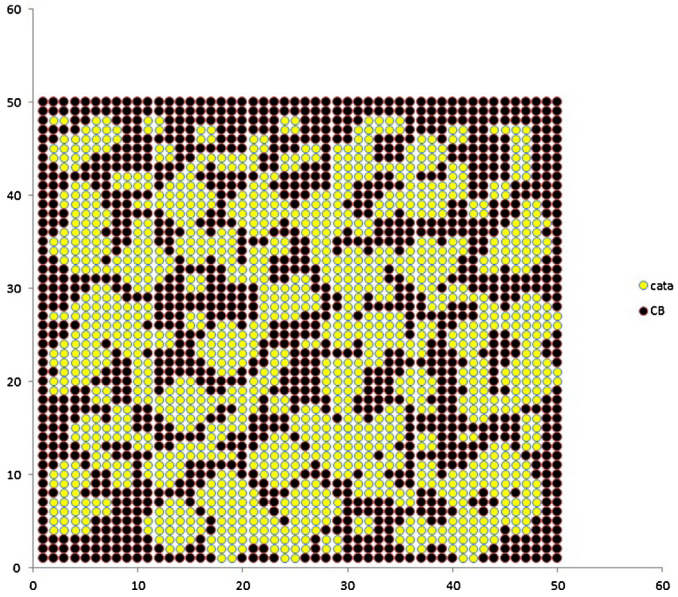

Fig. 7. Respective positions of the catalyst particles (yellow) and of the Carbon Black particles (black) for a sample with ratio 25CB–75CeO_2, at the height $z = 4$. (For interpretation of the references to colour in this figure legend, the reader is referred to the web version of this article.)

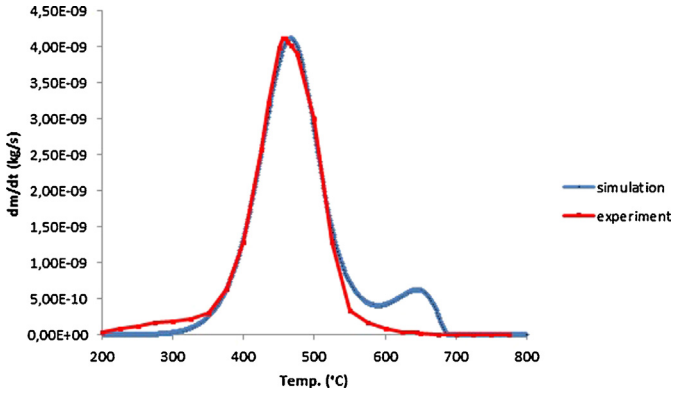

Fig. 8. The experimental (red) and simulated (blue) mass loss rate curves for almost catalytic reaction (mixture 25CB–75CeO_2). (For interpretation of the references to colour in this figure legend, the reader is referred to the web version of this article.)

We observe that a small extra peak occurring at around 620 °C is obtained in the simulated curve, after the main one which perfectly fits with the experimental peak. This means that the catalytic oxidation described in (1) is under-evaluated in our model. The extra peak corresponds to non-catalytic CB oxidation described in (2).

5.3. The case of a 50–50 medium

The placement of the CB particles and of the catalyst particles and aggregates is the same as in the case of a 25–75 mixture. The experimental and simulated mass loss rate curves are gathered in Fig. 9.

In this case, the further peak which occurs at around 650°C in the simulated curve has quite the same height than the first peak which is located at the same place (temperature) than in the experimental curve. Again the catalytic oxidation process (1) is largely under-evaluated in the model.

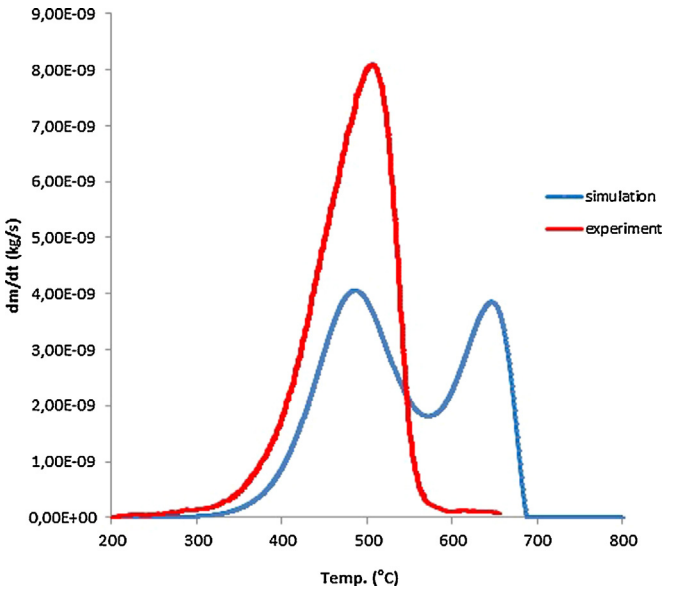

Fig. 9. The experimental (red) and simulated (blue) mass loss rate curves for a 50CB–50CeO_2 sample. (For interpretation of the references to colour in this figure legend, the reader is referred to the web version of this article.)

Table 4
Number of catalyst aggregates (200, 400, 800, 1200 nm) for each 3D bed considered for the parametric study (depending on the particle size distribution adopted for a 50–50 mass ratio mixture).

	Ref	A	B	C
200 nm	30	0	24	0
400 nm	159	300	0	1300
800 nm	93	100	248	0
1200 nm	30	25	0	0

5.4. Discussion

5.4.1. Changes in the constitution of the mixture

From the previous presentations concerning the mass loss rate curves for different mass ratios, one may conclude that the model which is presented here, with the above-indicated values of the kinetic constants, gives quite good results, except for the case of a 50–50 medium. In that case, the simulated curve presents two peaks of same importance which is quite far from the experimental observation.

A parametric study has been performed in this case of a 50–50 medium, in order to estimate the sensitivity of the model to the particle size distribution in the mixture. Hence, different 50–50 mixtures (hereafter referenced as Ref, A, B, C) have been considered whose characteristics are presented in Table 4. The mixture referenced as Ref is the one which has been previously described and studied. In the mixtures A, B and C we changed the numbers of the different types of aggregates.

A further distribution of the catalyst particles has also been studied for a 50–50 mass distribution, which consists to distribute the overall number of 200 nm catalyst particles in a random way throughout the bed and then to fill in the remaining free places of the bed with CB particles. We will call this distribution as random.

For these different mixtures (Ref, A, B, C and random), we obtain the simulated and experimental mass loss rate curves as gathered in Fig. 10.

There is no significant difference between the results obtained for the mixtures A and B, as the catalytic and the non-catalytic peaks occur at the same temperature and have quite the same size. For the mixture C, the non-catalytic peak is slightly smaller. This means

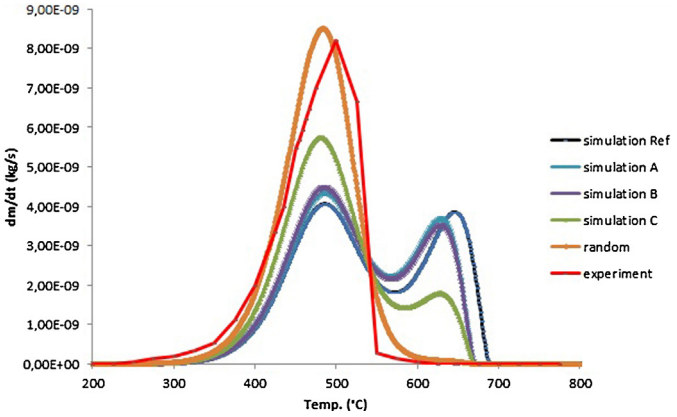

Fig. 10. Experimental and computed mass loss rate curves for a 50CB–50CeO_2 sample for different repartitions of the particles.

that whatever the distribution of the large particles in the mixture, the contact between CB and CeO_2 is quite similar and leads to very similar mass loss rate curves.

On the opposite, we clearly observe that when a random distribution of isolated catalyst particles is considered inside the bed, a very good approximation of the experimental curve is obtained.

From this parametric study, we can conclude that particle distributions with aggregates are relevant for the simulation of the media containing less than 50% of CeO_2. For higher ceria mass fraction in the mixture, the media defined with a random placement of small isometric volumes (200 nm) allow to simulate in an accurate way the catalytic oxidation of CB. It is difficult to give a clear explanation for this phenomenon. When preparing the mixtures, grinding step lasts exactly the same time for each sample. Hence, a decrease of the size of CeO_2 particles should result only on more robust media which allows breaking the largest ceria aggregates during a grinding process with more efficiency.

5.4.2. Changes in the values of the kinetic parameters

Our optimization process previously described suggests that for a 50–50 mass ratio mixture, the optimal value of the kinetic parameter k'_0 should be $k'_0 = 5300.2\ kg^{1-\alpha}\ s^{-1}$ instead of $k'_0 = 53.2\ kg^{1-\alpha}\ s^{-1}$ (factor 1000). When plugging this new value of k'_0 in the resolution of the problem (1)-(2), we indeed get a good superposition of the simulated and experimental mass loss curves. But plugging this value of k'_0 in the simulation of a 95–5 mass ratio mixture, we get a very poor superposition of the mass loss curves, as the simulated one starts very suddenly at around 450 °C while the experimental one starts in a more smooth way at 550 °C.

5.4.3. Changes in the distance of influence

An important parameter of our model is the distance of influence between CeO_2 and CB particles. Despite the numerous studies on catalytic carbon oxidation, the understanding of the solid to solid contact remains unclear. Only few studies were devoted to the analysis of the contact between soot and catalyst and the morphology of this contact [30]. In the present work, we assumed that only the neighbouring cells (sharing at least a summit) have to be considered for catalytic oxidation of CB to occur, but we have no experimental evidence for this assumption. In our model, the distance of influence ranges from 200 nm (denoted as a) to 346 nm (equal to $a\sqrt{3}$). If we change this maximal distance of influence to $2a\sqrt{3}$, thus taking more catalyst particles acting for the oxidation of a CB particle inside the bed, for a 50–50 mass ratio mixture, the two peaks which occur at a distance of influence equal to $a\sqrt{3}$ are joined in a unique

peak but which starts at lower temperatures (around 180 °C instead of 350 °C). In order to place this unique peak at the same place than the experimental one, we have to take $k_0 = 10\,000\ kg\ m^{-1}\ s^{-1}$ instead of $k_0 = 400\,000\ kg\ m^{-1}\ s^{-1}$ (dividing by 40!). But with this value of k_0 we then degrade the results concerning the other mass ratio mixtures.

5.4.4. Further discussion

Our model assumes that CB oxidation occurs without any change of the structure of the bed. Only the density of the CB particles decreases during the combustion process. Hence, the bed collapse during the reaction is not accounted for in our model. As a consequence, the contact between CB and CeO_2 is lost during reaction, especially for the CB particles which are surrounded by numerous CeO_2 particles. Consequently the catalytic CB oxidation is underestimated and the non-catalytic reaction is overestimated as shown for the 50–50 medium in Fig. 9. A model accounting for the collapse of the bed should improve significantly the results.

Nevertheless, once the model and the corresponding kinetic parameters are determined, it is possible to use them in order to test the influence of a catalyst (CeO_2 in this work) for different media or catalyst shapes.

6. Conclusion

Recently published works focused on the effect of the morphology and surface properties of CeO_2 based catalysts on soot oxidation [20], in order to maximize the number of contact points between soot and catalyst surface. Beside such experimental works, modelling is a relevant way to investigate the effect of the contact between soot and catalyst materials. In a previous work [16], we proposed a global model for Carbon Black (CB) oxidation in the presence of cerium oxide. In the current paper, we proposed a refined model for catalytic carbon oxidation which is based on a 3D representation of mixtures involving CB and commercial ceria (CeO_2) particles. This model is a robust tool for the optimization of the shape and the size of the catalyst used for carbon oxidation. It allows extracting the kinetic parameters of CB oxidation within this context. The simulated values of the rate of carbon oxidation in a fixed bed reactor are well predicted for different CB/CeO_2 ratios, except for the 50–50 mass ratio, for which the contact is lost during combustion, as the collapse of the bed is not simulated in this model.

In order to take into account this phenomenon, a model accounting for the bed collapse is currently under development in our laboratory. Further experiments should be done in the next future with other catalysts (type, structure, size) in order to test the validity of our model.

Acknowledgements

We thank Prof. Corinne Petit from ICPEES University of Strasbourg, especially for the microscope photography of Fig. 1. We also thank Prof. Hakim Mahzoul from LGRE who contributed to the preparation of the PhD [28]. We also thank the network REALISE (REseau Alsace de Laboratoires en Ingénierie et Sciences pour l'Environnement) for the financial support to equipment facilities.

References

[1] B.A.A.L. van Setten, M. Makkee, J.A. Moulijn, Catal. Rev. Sci. Eng. 43 (2001) 489–564.
[2] S. Wagloehner, S. Kureti, Appl. Catal. B 129 (2013) 501–508.
[3] M. Schejbal, J. Stepanek, M. Marek, P. Koci, M. Kubicek, Fuel 89 (2010) 2365–2375.
[4] Y. Teraoka, K. Nakano, S. Kagawa, W.F. Shanguan, Appl. Catal. B 5 (3) (1995) 181–185.
[5] C.B. Lim, H. Kusaba, H. Einaga, Y. Teroka, Catal. Today 175 (2011) 106–111.
[6] A. Bueno-Lopez, Appl. Catal. B 146 (2014) 1–11.
[7] A. Bueno-Lopez, K. Krishna, M. Makkee, J.A. Moulijn, J. Catal. 230 (2005) 237–248.
[8] E. Aneggi, M. Boaro, C. de Leitenburg, G. Dolcetti, A. Trovarelli, J. Alloys Compd. 408–412 (2006) 1096–1112.
[9] G. Mul, F. Kapteijn, C. Doornkamp, J. Moulijn, J. Catal. 179 (1998) 258–266.
[10] N. Guillen-Hurtado, A. Garcia-Garcia, A. Bueno-Lopez, Appl. Catal. B 174 (2015) 60–66.
[11] A. Laachir, V. Perichon, A. Badri, J. Lamotte, E. Catherine, J.C. Lavalley, et al., J. Chem. Soc. Faraday Trans. 87 (10) (1991) 1601–1609.
[12] P. Fornasiero, J. Kaspar, T. Montini, M. Graziani, V. Dal Santo, R. Psaro, S. Recchia, J. Mol. Catal. A: Chem. 204–205 (2003) 683–691.
[13] M. Boaro, F. Giordano, S. Recchia, V. Dal Santo, M. Giona, A. Trovarelli, Appl. Catal. B 52 (2004) 225–237.
[14] G. De Soete, in: Western States section meeting of the Combustion Institute, Salt Lake City.
[15] G.A. Stratakis, A.M. Stamatelos, Combust. Flame 132 (2003) 157–169.
[16] M. Issa, C. Petit, A. Brillard, J.-F. Brilhac, Fuel 87 (2008) 740–750.
[17] B.A.A.L. van Setten, J.M. Schouten, M. Makkee, J.A. Moulijn, Appl. Catal. B 28 (2000) 253–257.
[18] S. Bensaid, N. Russo, D. Fino, Catal. Today 216 (2013) 57–63.
[19] M. Issa, C. Petit, H. Mahzoul, J.-F. Brilhac, A. Aboukais, Top. Catal. 52 (13–20) (2009) 2063–2069.
[20] P. Miceli, S. Bensaid, N. Russo, D. Fino, Chem. Eng. J. 278 (2015) 190–198.
[21] D. Fino, N. Russo, G. Saracco, V. Specchia, J. Catal. 217 (2003) 367–375.
[22] D. Fino, N. Russo, G. Saracco, V. Specchia, J. Catal. 242 (2006) 38–47.
[23] B.R. Stanmore, J.-F. Brilhac, P. Gilot, SAE Paper 010115, 1999.
[24] K. Leistner, A. Nicolle, D. Berthout, P. da Costa, Combust. Flame 159 (2012) 64–76.
[25] K. Yamamoto, S. Oohori, H. Yamashita, S. Daido, Proc. Combust. Inst. 32 (2009) 1965.
[26] N.V. Vernikovskaya, T.L. Pavlova, V.V. Mokrinskii, D. Yu Murzin, N.A. Chumakova, Chem. Eng. J. 269 (2015) 416–424.
[27] A. Rougier, S. Soiron, I. Haihal, L. Aymard, B. Taouk, J.-M. Tarascon, Powder Technol. 128 (2–3) (2002) 139–147.
[28] M. Issa, Thèse de l'Université de Haute-Alsace, 2008.
[29] T. Ozawa, J. Therm. Anal. Calorim. 7 (1975) 601–617.
[30] A. Setiabudi, N.K. Allart, M. Makkee, J.A. Moulijn, Appl. Catal. B 60 (3–4) (2005) 233–243.
[31] M. Issa, C. Petit, H. Mahzoul, A. Brillard, J.-F. Brilhac, SAE Technical Paper Series 2007-24-0091.